Materials Research. 2023; 26(suppl. 1):e20220585
DOI: https://doi.org/10.1590/1980-5373-MR-2022-0585

Effects of Mn Concentration on Grain Boundary Pinning of 5083 Aluminum Alloy

***Caio F.S. Gomes*[a], *André da S. Antunes*[a*]**

[a]*Instituto Tecnológico de Aeronáutica (ITA), Departamento de Materiais e Processos, Praça Marechal-do-Ar Eduardo Gomes, 50, CEP 12245-021, São José dos Campos, SP, Brasil.*

Received: December 16, 2022; Revised: April 28, 2023; Accepted: May 25, 2023

Superplastic deformation has a significant industrial application value due to the large elongation, which allows manufacturing parts with complex geometries but happens at elevated temperatures and low strain rates. Therefore, it requires alloys with fine grain size but whose grains tend to grow at processing temperatures. Second-phase particles can promote grain boundary pinning to keep a fine grain size structure during superplastic forming. In 5083 aluminum alloy, Al_6Mn particles make grain boundary pinning. There are two types of 5083 aluminum alloy: conventional with manganese range from 0.4 to 1.0 wt.% and superplastic with manganese between 0.64 and 0.86. It was observed in bibliographic research that the 5083 superplastic has a higher chemical concentration of manganese than the conventional one. However, no references were found covering manganese concentration in grain size stability. This work shows grain size evolution at a constant temperature of 5083 alloys with different manganese concentrations. This work indicates that the manganese substantially impacts grain boundary pinning when the chemical composition is between 0 and 0.6 wt.%. No significant effects were observed for Mn concentrations higher than 0.6%".

Keywords: *Aluminum Alloys, superplasticity, AA 5083, grain boundary pinning.*

1. Introduction

The mobilization of the governments to achieve the CO2 emission reduction targets determined in international conferences such as COP26 has pressed corporations of all sectors to adopt definitions and strategies concerning the ESG Agenda. It is often reflected in the search for more efficient processes and less polluting raw materials for the industrial environment. In this context, the automotive industry sees the substitution of steel for aluminum alloys in automotive vehicle fairings manufacturing as an alternative.

Aluminum alloys show advantages over steel in reducing CO2 emission because of their lower specific weight, better aerodynamics, and the economy in the assembly of automobiles. The last two factors are related to the feasibility of producing parts with complex geometry that improve aerodynamics and still save time and energy in assembly, reducing the need for welding and riveting[1,2]. The advantages are even more significant for aluminum alloys with a superplastic character.

Superplasticity is the capacity of certain materials to exhibit high elongation before failure, allowing the manufacture of parts with complex geometry with a reduced number of steps or intermediate heat treatment processes[3]. Typical superplastic elongations are higher than 300%, but some metal alloys can overcome 5,000%[4].

The phenomenon of superplasticity typically occurs by deformation via grain boundary sliding rather than via dislocation slip. Since grain boundary sliding is a surface phenomenon, it requires fine or ultrafine grain size[5,6]. However, the phenomenon demands high working temperatures and low strain rates, which are known to induce grain growth due to the prolonged times in elevated temperatures[3-7]. So, grain growth kinetics is an essential subject in the superplasticity area[8-10].

To solve this trade-off, chemical elements in alloy manufacturing keep the grain size small even at high temperatures for a prolonged time. These elements can form stable particles, commonly originating during solidification, that may act as grain boundary pinning[7-11]. By that, the grain growth rate is reduced to stabilize the grain size even in a prolonged time of tens of hours.

The 5083 SP aluminum alloy, well established in the industry, has superplastic characteristics stretching around 350%. Since its first application in 1986, thousands of components have been produced, and there are several sheet manufacturers of this alloy, mainly in the USA, Europe, and Japan[12]. The primary particle that pins the grain boundary in this alloy is Al_6Mn[13,14]. Therefore, manganese is a critical component for the exhibition of the superplastic phenomenon in that case.

ASTM regulates that manganese concentration in the conventional 5083 aluminum alloy varies between 0.4 and 1.0 wt.%[15]. On the other hand, a bibliographic survey showed that the 5083 superplastic aluminum alloy has a narrower range for the Mn concentration, between 0.64 and 0.86 wt.%[16]. However, no reports explaining the different Mn concentrations for the 5083 SP and conventional 5083 aluminum alloys were found in the consulted literature. Therefore, this work aims to evaluate the influence of Mn concentration on the grain growth behavior of 5083 aluminum alloy to answer that literature gap.

*e-mail: antunes@ita.br

2. Experimental Section

Five AA 5083 alloys with different Mn concentrations were produced from primary aluminum and the following master alloys: Al with 35.0 wt.% of Mg, Al with 17.4 wt.% of Mn, and Al with 12.0 wt.% of Si. At first, the primary aluminum was melted and held at 750 ºC using a resistance metal melting furnace, and 15 ppm of Be was added to avoid magnesium oxidation. Then, the master alloys were added and kept for 15 min. After it, the melting baths were degassed using Hexachloroethane, and then they were poured into a water-cooled copper crucible with 127 x 54 x 13 mm. The nominal compositions are presented in Table 1.

The ingots were machined to remove superficial defects and improve the rolling quality. Then, they were submitted to homogenization heat treatment at 500 ºC for 8 h. Ingots were hot sheet rolled at 420 ºC to 13,75 mm in thickness and cold-rolled at room temperature to 2.5 mm, resulting in 81.8% of work hardening. Next, the sheets were annealed at 350ºC for 30 minutes, and they were cut into samples of 1 cm × 1 cm and submitted at 450 ºC for 0 (untreated), 1, and 4 h to investigate grain growth. The 1-hour time frame was selected as it represents the time taken for the sheet to reach thermal equilibrium with the furnace, while the 4-hour time frame was chosen as it usually takes that time to shape a superplastic sheet, including the 1 hour previously mentioned. Finally, the samples were heat-treated at 130 ºC for 15 h to decorate grain boundaries with the Mg2Si etchable phase.

After the usual metallographic preparation, the samples were etched in an aqueous acid solution containing 10 vol.% phosphoric acid at 50 ºC per 15 min. Finally, the samples were observed in an optical microscope. Following the standard ASTM E112-13(2021), the Lineal Intercept Procedure was applied to 5 images at each condition to obtain the grain sizes.

Samples were analyzed by X-ray diffractometry, using a PANalytical Empyrean, with Cu target (Kα radiation 1.5418 Å). Crystallite sizes were measured using the Scherrer Equation without a standard. Thus, the values of crystallite size are semiquantitative.

Statistical analysis was based on a 2k factorial design with k = 2 factors with replication ($2.2^2 = 8$ experiments). Table 2 presents the experimental design used in the study, consisting of two parameters that were varied between low and high levels. The parameters were manganese concentration and grain growth time, and they were denoted by -1 and 1, respectively. The experimental design included eight experiments, with each experiment representing a different combination of the low and high levels of the two parameters.

The dataset in the Table 2 was organized by analysis. For analysis 1, the points (1, 0), (1, 0.4), (4, 0), and (4, 0.4) were used, where the first digit indicates the grain growth time in hours, while the second digit represents the manganese concentration in weight percentage (wt.%). For analysis 2, the points (1, 0.4), (1, 0.6), (4, 0.4), and (4, 0.6) were used. For analysis 3, the points (1, 0.6), (1, 0.8), (4, 0.6), and (4, 0.9) were used. Finally, for analysis 4, the points (1, 0.8), (1, 1.0), (4, 0.8), and (4, 1.0) were used. This approach allowed for a more detailed analysis of the data and a better understanding of the relationship between the variables. Linear regression models were used to establish the relationship between grain size and manganese concentration and grain growth time at 450ºC for each analysis.

3. Results and Discussion

Figure 1 shows some examples of optical microscopy images obtained from AA 5083 samples at different manganese concentrations and grain growth times. These images were used for the analysis of grain size, which was used to develop linear regression models to establish the relationship between grain size, manganese concentration, and grain growth time at 450ºC.

Table 3 shows the grain size as a function of the manganese concentration of AA 5083 after annealing and before grain growth treatment. It can be observed that the manganese is efficient in diminishing de initial grain size. However, the main focus of this work is to evaluate the grain growth resistance (i.e., grain boundary pinning) at 450ºC.

Samples of AA 5083 with different manganese concentrations were annealed and submitted to heat treatment at 450ºC per 1 and 4 h to study the grain growth behavior. Linear regressions were performed using de following equation: $G = \beta 0 + \beta 1.Mn + \beta 2.t + \beta 12.Mn.t$. Were G is the grain size, Mn is the chemical composition of manganese in weight percent and t is the grain growth time. Table 4 shows the estimated coefficients, the standard deviations, the t-values (estimate), the Shapiro-Wilk tests, and the adjusted R^2 for the four manganese concentrations ranging from 0 to 0.4 (analysis 1), 0.4 to 0.6 (analysis 2), 0.6 to 0.8 (3), and 0.8 to 1.0 (4).

Table 1. Nominal chemical compositions of AA 5083 with different manganese concentrations.

Sample	Mn / wt.%	Mg / wt.%	Si / wt.%
1	0.0	4.6	0.3
2	0.4	4.6	0.3
3	0.6	4.6	0.3
4	0.8	4.6	03.
5	1.0	4.6	03.

Table 2. Experimental design consisting of two parameters varying between low and high levels, -1 and 1, respectively.

EXPERIMENT	Mn	Grain growth time
1	-1	-1
2	1	-1
3	-1	1
4	1	1
5	-1	-1
6	1	-1
7	-1	1
8	1	1

Table 3. Grain size as a function of manganese concentration of AA 5083 after annealing and before grain growth treatment.

Mn/ wt.%	Grain size/ µm	STD. ERROR
0	12.77	1.54
0.4	9.02	0.75
0.6	7.64	0.92
0.8	6.88	0.28
1.0	6.48	0.49

For this study, p-values lower than 0.05 were considered statistically significant and are shown in bold. Normality can be observed in all analyses, as every p-value for the Shapiro-Wilk normality test is higher than 0.05, indicating that the null hypothesis (normality) can be assumed. In addition, the values of adjusted R^2 are high, so the linear model is significant[17].

The manganese concentration was the most influential parameter in analyses 1 and 2 (manganese ranging from 0 to 0.6). However, its parameter is almost zero and is not statistically relevant in manganese ranging from 0.6 to 1 (analyses 3 and 4). Nevertheless, it shows that the influence of manganese in pinning the grain growth diminishes with its concentration.

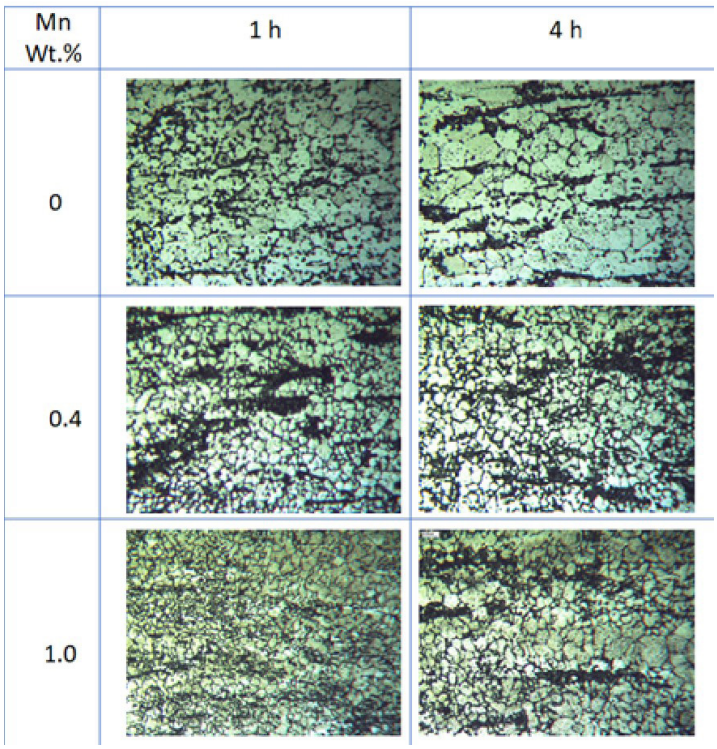

Figure 1. Optical microscopy images of AA 5083 samples at various manganese concentrations and grain growth times resulting from the experimental design presented in Table 2.

Table 4. Statistical analysis of the main effects and interactions for the four analyses. Statistically relevant values (p-value < 0.1) are bolded. Also shown are the estimated coefficients, the standard deviations, and the t-values (estimate). The Shapiro-Wilk tests are shown and used to determine de regressions' adequation.

ANALYSE	B	ESTIMATE	STD. ERROR	T-VALUE	P-VALUE (ESTIMATE)	ADJ. R^2	P-VALUE (SHAPIRO-WILK)
1 0 to 0.4 wt.%Mn	β0	16.316	0.233	70.028	2.49e-07	0.98	0.8789
	β1	-4.346	0.233	-18.653	4.86e-05		
	β2	1.075	0.233	4.616	0.00991		
	β12	-1.048	0.233	-4.497	0.01084		
2 0.4 to 0.6 wt.%Mn	β0	10.783	0.096	112.489	3.75e-08	0.97	0.6084
	β1	-1.187	0.096	-12.384	0.000244		
	β2	0.505	0.096	5.267	0.006225		
	β12	0.477	0.096	4.979	0.007602		
3 0.6 to 0.8 wt.%Mn	β0	9.293	0.195	47.699	1.16e-06	0.80	0.7973
	β1	-0.303	0.195	-1.555	0.19502		
	β2	1.041	0.195	5.342	0.00592		
	β12	0.059	0.195	0.301	0.77875		
4 0.8 to 1.0 wt.%Mn	β0	9.164	0.199	46.155	1.32e-06	0.82	0.6859
	β1	0.174	0.199	0.876	0.43047		
	β2	1.168	0.199	5.885	0.00417		
	β12	0.069	0.199	0.349	0.74496		

Figure 2 shows the main parameter effects (a-b) and interactions (c-f) plots for the grain size variation. The extremities of each line indicate the average grain size when the parameter is at a given level. However, the effect is not necessarily statistically relevant, as shown in Table 4. In the Figure 2 a), x-axis is normalized with -1 and 1 representing the lower and higher levels of manganese concentration, respectively, for each analysis, as there are different concentrations of manganese in each line.It is shown that manganese has a substantial impact on grain boundary pinning when the chemical composition is between 0 and 0.6 wt.%, as the slope of the line is very steep. However, there are no significant effects when the manganese concentration is above 0.6 wt.%, as the lines become horizontal, as shown in orange and red. It can be seen in Figure 2 b) that grain size grows with time in every manganese range.

Figure 2 (c-f) shows the interaction effects, which can be interpreted as follows. When the lines are concurrent, the independent variables (manganese concentration and time) interact to create a specific combined effect for the dependent variable (grain size); when they are parallel, the independent variables do not exhibit a combined effect. Thus, the increasing manganese concentration affects the behavior of grain growth between 0 and 0.6 wt.% Mn. However, adding manganese above 0.6 wt.% does not improve the grain boundary pinning. Its behavior can be visualized in the grain size contour map as a function of manganese concentration and time, shown in Figure 3, obtained in the linear regression model.

The Zener pinning pressure that restricts grain growth depends on the size and fraction of second-phase particles. The higher the fraction and the smaller the particle size, the better this effect. It was expected that increasing the manganese concentration would increase the fraction and improve the grain boundary pinning. Still, the results show that adding manganese above 0.6 wt.% does not improve the grain boundary pinning. It was suspected that the second phase particle size increases with manganese concentration.

Figure 4 shows the x-ray diffraction pattern (XRD) of AA 5083 at different manganese concentrations. The peaks related to phases Al_6Mn appear with the addition of manganese. The crystallite size and fraction as a function of manganese concentration are presented in Figure 5. It can be seen that the fraction of Al_6Mn increases with manganese concentration, which is suitable for grain boundary pinning. However, the crystallite size increases with manganese concentration. It indicates that adding manganese above 0.6 wt.% does not improve the grain boundary pinning because the Al_6Mn particle size increases. As the liquidus temperature rises with manganese concentration[18], it is suspected that the increase in manganese concentration causes an increase in the coarse particles of Al_6Mn precipitated in the melting pool. Then, increasing the melting pool temperature is suggested.

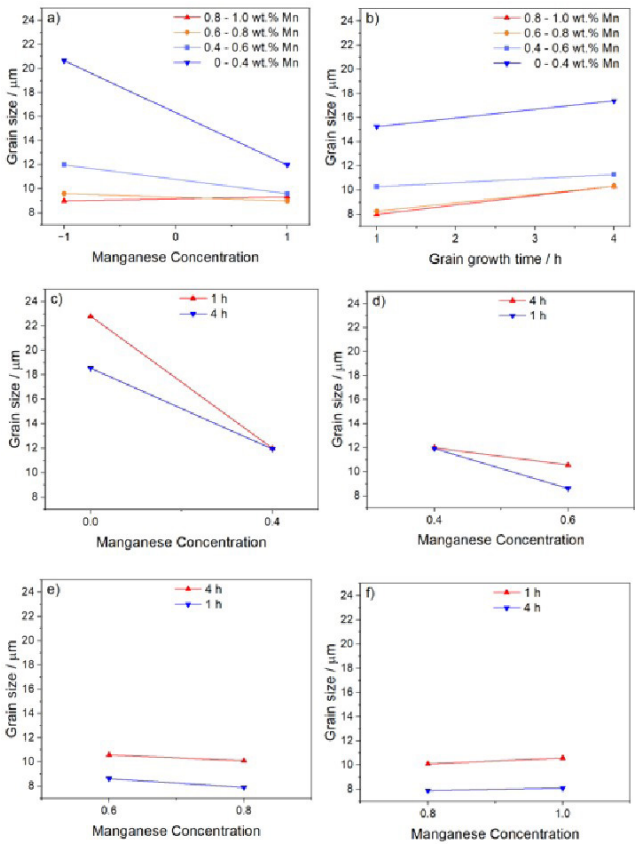

Figure 2. Main parameter effects (a-b) and interactions (c-f) , analysis 1 to 4, plots for the grain size variation with manganese concentration and grain growth time at 450 ºC of AA 5083. The extremities of each line indicate the average grain size when the parameter is at a given level. The effect is not necessarily statistically relevant, as shown in Table 4.

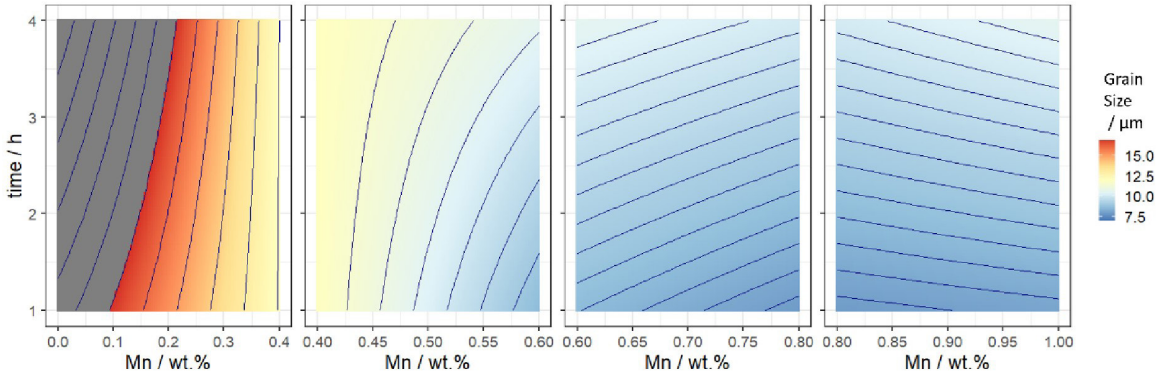

Figure 3. Grain size contour map as a function of manganese concentration and grain growth time at 450 ºC of AA 5083.

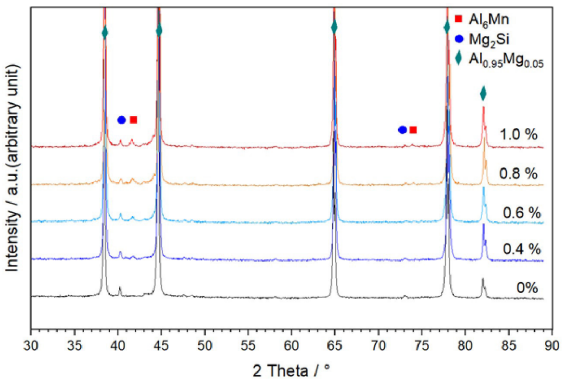

Figure 4. X-ray diffraction pattern (XRD) of AA 5083 at different manganese concentrations.

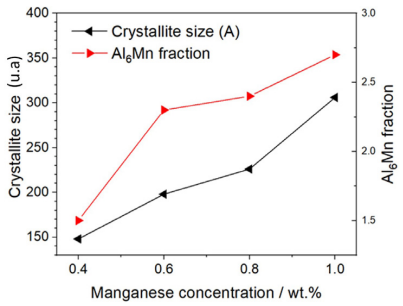

Figure 5. Crystallite size and fraction as a function of manganese concentration of the AA 5083.

4. Conclusions

In conclusion, this study investigated the influence of manganese concentration on microstructural refinement and grain boundary pinning of AA 5083 aluminum alloy. The results showed that adding manganese up to 0.6 wt.% decreases the initial grain size and improves the grain boundary pinning. However, adding manganese above 0.6 wt.% does not improve the grain boundary pinning due to the increase in Al6Mn particle size. The linear regression models established the relationship between grain size, manganese concentration, and grain growth time at 450ºC. The statistical analysis of the main effects and interactions for the four manganese concentrations ranging from 0 to 1.0 wt.% revealed that the manganese concentration was the most influential parameter. Moreover, the grain size contour map obtained from the linear regression model shows the effect of manganese concentration and time on grain size variation. Finally, XRD analysis showed that the addition of manganese increases the fraction of Al6Mn suitable for grain boundary pinning, but the increase in the particle size of Al6Mn particles diminishes the pinning effect. These findings are significant in understanding the effects of manganese concentration on grain refinement and optimizing the alloy's superplastic properties. Future research should focus on analyzing the effects of manganese concentrations on strain-rate sensitivity coefficient (m), ductility, and cavitation in 5083 alloys.

5. Acknowledgments

The authors thank the following organizations for making this project possible: Alfa Trend Indústria e Comércio Ltda; and ITAEx - Ex-Alunos Apoiando o ITA.

We thank the Laboratory of Plasma and Processes of the Instituto Tecnológico de Aeronáutica for providing the XRD analyses.

6. References

1. Pereira DA, Batalha MHF, Carunchio AF, Resende HB. An analysis of superplastic forming to manufacture aluminum and titanium alloy components. In: Aerospace Technology Congress. Proceedings. São Paulo: Fundação de Apoio ao IPT; 2016. p. 1-13.
2. Majidi O, Jahazi M, Bombardier N. Finite element simulation of high-speed blow forming of an automotive component. Metals (Basel). 2018;8(11):901. http://dx.doi.org/10.3390/met8110901.
3. Langdon TG. Seventy-five years of superplasticity: historic developments and new opportunities. J Mater Sci. 2009;44(22):5998-6010.
4. Higashi K, Ohnishi T, Nakatani Y. Superplastic behavior of commercial aluminum bronze. Scr Metall. 1985;19:821-3.
5. el al Bhatta L. Recent development of superplasticity in aluminum alloys: a review. Metals (Basel). 2020;10(77):1-26.
6. Bobruk EV, Sauvage X, Enikeev NA, Valiev RZ. Influence of fine scale features on room temperature superplastic behaviour of an ultrafine-grained Al-30Zn alloy. Mater Lett. 2019;254:329-31. http://dx.doi.org/10.1016/j.matlet.2019.07.097.

7. Kaibyshev OA. Superplasticity of alloys, intermetallides and ceramics. New York: Springer-Verlag; 1992. 317p.
8. Reed-Hill RE, Abbaschian R, Abbaschian L. Physical metallurgy principles. 4. ed. Stamford: Cengage Learning; 2008.
9. Nokhrin AV, Gryaznov MY, Shotin SV, Nagicheva GS, Chegurov MK, Bobrov AA, et al. Effect of Sc, Hf, and Yb additions on superplasticity of a fine-grained Al-0.4%Zr alloy. Metals (Basel). 2023;13(1):133. http://dx.doi.org/10.3390/met13010133.
10. Mosleh AO, Yakovtseva OA, Kishchik AA, Kotov AD, Moustafa EB, Mikhaylovskaya AV. Effect of coarse eutectic-originated particles on the microstructure and properties of the friction stir-processed Al-Mg-Zr-Sc-based alloys. J Miner Met Mater Soc. 2023. Online. http://dx.doi.org/10.1007/s11837-023-05712-x.
11. Lee SW, Yeh JW. Superplasticity of 5083 alloys with Zr and Mn additions produced by reciprocating extrusion. Mater Sci Eng A. 2007;460-461:409-19.
12. Barnes AJ, Raman H, Lowerson A, Edwards D. Recent application of superformed 5083 aluminum alloy in the aerospace industry. Mater Sci Forum. 2012;735:361-71. http://dx.doi.org/10.4028/www.scientific.net/MSF.735.361.
13. Engler O, Miller-Jupp S. Control of second-phase particles in the Al-Mg-Mn alloy AA 5083. J Alloys Compd. 2016;689:998-1010.
14. Mironov S, Malopheyev S, Vysotskiy I, Kaibyshev R. Superplasticity of friction-stir welds of Zr-modified 5083 aluminum alloy with ultrafine-grained structure. Defect Diffus Forum. 2018;385:15-20. http://dx.doi.org/10.4028/www.scientific.net/DDF.385.15.
15. ASTM: American Society for Testing and Materials. ASTM B209-14: standard specification for aluminum and aluminum alloy sheet and plate. West Conshohocken: ASTM; 2014.
16. Antunes AS, Tosetti JPV. Superplasticidade na liga de alumínio 5083. Columbia: KDP; 2020. (Portuguese Edition)
17. Montgomery D. Design and analysis of experiments. New York: John Wiley; 2013.
18. Shukla A, Pelton AD. Thermodynamic assessment of the Al-Mn and Mg-Al-Mn systems. J Phase Equilibria Diffus. 2009;30(1):28-39. http://dx.doi.org/10.1007/s11669-008-9426-5.